Cellular and Molecular Life Sciences (2023) 80:156
https://doi.org/10.1007/s00018-023-04798-5

ORIGINAL ARTICLE

CSNK1D-mediated phosphorylation of HNRNPA2B1 induces miR-25-3p/miR-93-5p maturation to promote prostate cancer cell proliferation and migration through m^{6}A-dependent manner

Feng Qi[1] · Wenyi Shen[2] · Xiyi Wei[3] · Yifei Cheng[4] · Fan Xu[5] · Yuxiao Zheng[1] · Lu Li[6,7] · Chao Qin[3] · Xiao Li[1,8]

Received: 13 January 2023 / Revised: 18 April 2023 / Accepted: 4 May 2023 / Published online: 19 May 2023

Abstract

It has been reported that heterogeneous nuclear ribonucleoprotein A2/B1 (HNRNPA2B1) is highly expressed in prostate cancer (PCa) and associated with poor prognosis of patients with PCa. Nevertheless, the specific mechanism underlying HNRNPA2B1 functions in PCa remains not clear. In our study, we proved that HNRNPA2B1 promoted the progression of PCa through in vitro and in vivo experiments. Further, we found that HNRNPA2B1 induced the maturation of miR-25-3p/miR-93-5p by recognizing primary miR-25/93 (pri-miR-25/93) through N6-methyladenosine (m^{6}A)-dependent manner. In addition, both miR-93-5p and miR-25-3p were proven as tumor promoters in PCa. Interestingly, by mass spectrometry analysis and mechanical experiments, we found that casein kinase 1 delta (CSNK1D) could mediate the phosphorylation of HNRNPA2B1 to enhance its stability. Moreover, we further proved that miR-93-5p targeted BMP and activin membrane-bound inhibitor (BAMBI) mRNA to reduce its expression, thereby activating transforming growth factor β (TGF-β) pathway. At the same time, miR-25-3p targeted forkhead box O3 (FOXO3) to inactivate FOXO pathway. These results collectively indicated that CSNK1D stabilized HNRNPA2B1 facilitates the processing of miR-25-3p/miR-93-5p to regulate TGF-β and FOXO pathways, resulting in PCa progression. Our findings supported that HNRNPA2B1 might be a promising target for PCa treatment.

Keywords Prostate cancer · HNRNPA2B1 · m^{6}A · CSNK1D

Feng Qi, Wenyi Shen, Xiyi Wei and Yifei Cheng have contributed equally to this work.

✉ Xiao Li
leex91@163.com

✉ Chao Qin
qinchao@njmu.edu.cn

Feng Qi
qf199408@163.com

[1] Department of Urologic Surgery, Jiangsu Cancer Hospital and Jiangsu Institute of Cancer Research and Affiliated Cancer Hospital of Nanjing Medical University, Nanjing 210009, China

[2] Department of Hematology, The First Affiliated Hospital of Nanjing Medical University, Nanjing, China

[3] State Key Laboratory of Reproductive Medicine, Department of Urology, The First Affiliated Hospital of Nanjing Medical University, Nanjing 210029, China

[4] Department of Urology, The First Affiliated Hospital of Nanjing Medical University, Nanjing 210029, China

[5] Jiangsu Cancer Hospital & Jiangsu Institute of Cancer Research & Affiliated Cancer Hospital of Nanjing Medical University, Nanjing 210009, China

[6] State Key Laboratory of Translational Medicine and Innovative Drug Development, Jiangsu Simcere Diagnostics Co., Ltd, Nanjing, China

[7] Nanjing Simcere Medical Laboratory Science Co., Ltd, Nanjing, China

[8] Department of Scientific Research, Jiangsu Cancer Hospital and Jiangsu Institute of Cancer Research and Affiliated Cancer Hospital of Nanjing Medical University, Nanjing, China

Introduction

Prostate cancer (PCa) is a very common malignancy occurring particularly in elderly males, with approximately 174,650 new cases and 31,620 deaths per year in the USA, according to the 2019 estimates of the American Cancer Society [1]. Despite the treatment options such as surgery and radiation therapy are currently available for PCa patients, the 5-year survival rate for patients in advanced stage is still poor [2]. Therefore, a better understanding of the mechanisms underlying PCa development is urgently required.

RNA modifications are involved in the development of human diseases, including cancers. Recent studies reveal that N6-methyladenosine (m^6A) modification is the most extensive modification in the progression of different cancers [3]. The formation and regulation of m^6A are manipulated by a methyltransferase complex comprising three categories of proteins, including "readers", "writers" and "erasers" [4]. Heterogeneous nuclear ribonucleoprotein (HNRNP) protein families, including HNRNPC and HNRNPA2B1, are m^6A reader proteins which can interpret m^6A methylation and drive downstream functional signals [5]. Moreover, HNRNPA2B1 can mediate m^6A-dependent nuclear RNA processing [6]. As reported previously, HNRNPA2B1 is overexpressed in various malignancies, such as head and neck cancer [7], ovarian cancer [8] and breast cancer [9]. Of note, a study proposed by Jacqueline Stockley et al. has pointed that HNRNPA2B1 is overexpressed in PCa [10]. Besides, it has been reported that high expression of HNRNPA2B1 is associated with poor prognosis of PCa [11]. However, the specific mechanism underlying HNRNPA2B1 functions in PCa is not clear.

As a small type of endogenous non-coding RNA consisting of 21–24 nucleotides, microRNAs (miRNAs) have been recognized as key regulators of many biological processes [12]. MiRNAs are initially transcribed as primary miRNAs (pri-miRNAs) which are then cut into hairpin-structured precursor miRNAs (pre-miRNAs). Pre-miRNAs are processed to form mature miRNAs that actually exert the functions [13]. MiRNAs usually function at the post-transcriptional level either by inhibiting messenger RNA (mRNA) translation or by promoting mRNA degradation [14]. Many evidences have demonstrated that miRNAs are potential diagnostic, prognostic, and therapeutic biomarkers for PCa [15].

Transforming growth factor-beta (TGF-β) plays a crucial role in the pathophysiology of cancers. TGF-β family members cooperate with membrane receptor serine–threonine protein kinase, leading to the activation of Smad transcription factors (TFs) [16]. The activation of the TGF-β signaling can promote PCa progression [17].

Forkhead box transcription factors (FOXO) family belongs to growth factor and stress regulated transcription factors. FOXOs are involved and implicated in multiple cellular functions, including differentiation, apoptosis and proliferation [18]. Increasing evidences have revealed that dysregulation of FOXO proteins is related to the progression of cancers, including PCa [19].

In our study, we investigated the tumor-promoting role of HNRNPA2B1 in PCa. Besides, we explored the interaction between casein kinase 1 delta (CSNK1D) and HNRNPA2B1 as well as the maturation of miR-25-3p/miR-93-5p induced by HNRNPA2B1-recognized m^6A site.

Materials and methods

Clinical samples and tissue microarray analysis

This study was approved by the Institutional Review Board of the First Affiliated Hospital of Nanjing Medical University. All patients participated in the study voluntarily donated samples for clinical research and signed informed consents before surgery. Samples were collected from pathologically diagnosed patients with prostate adenocarcinoma who underwent radical prostatectomy in the Department of Urology Department of the First Affiliated Hospital of Nanjing Medical University from September 2008 to January 2014. Samples (PCa tissue and matching normal prostate tissue) were collected under the guidance of an experienced pathologist, and immediately stored in a liquid nitrogen tank. The collected samples were made into tissue microarray and stored in a 4℃ refrigerator for subsequent use. Immunohistochemistry (IHC) was used to detect the expression level of HNRNPA2B1. The brown area represented the positivity of HNRNPA2B1 expression. The staining area accounts for below 25% of total area was considered low HNRNPA2B1 expression, while more than 25% was considered high HNRNPA2B1 expression. We collected the basic characteristics and clinicopathological features of all patients, and followed up the patients every 6 months. We collected surgical specimens from 240 PCa patients and made them into tissue chips. After screening, 151 patients were ultimately included for analysis. The exclusion criteria were as follows: 29 patients lacked clinically important information (including prostate-specific antigen (PSA), TNM staging, etc.), 35 patients were lost or unwilling to cooperate during the follow-up process and 25 patients failed IHC staining. The relationship between the HNRNPA2B1 expression and clinicopathological features or biochemical recurrence-free survival (bRFS) was analyzed using chi-square test or Kaplan–Meier method. Finally, univariate and multivariate Cox Regression model was constructed to investigate the independent prognostic factors for bRFS.

Cell culture

PCa cells (PC3 and DU145) and human normal prostate epithelial cell (RWPE-1) were purchased from ATCC (Manassas, VA, USA) and cultured in RMI1640 medium (CD-02168-ML, GIBCO, USA) supplemented with 10% fetal bovine serum (10270–106, GIBCO, USA) and 100 U/mL penicillin/streptomycin and stored in a humidifier chamber containing 5% CO_2 at 37 ℃.

RT-qPCR

Total RNA was isolated from PCa cells using TRIzol reagent (abs60154, absin, China). cDNA was synthesized using the Prime Script™ RT Reagent Kit (11141ES10, Takara, Japan), and then qPCR was performed with the SYBR Green qPCR Master Mix kit (QR0100-1KT, Sigma-Aldrich, USA). Gene expression was evaluated using the $2^{-\Delta\Delta Ct}$ method. GAPDH and U6 were used as internal control genes.

Cell transfection

Three specific shRNAs targeting HNRNPA2B1 (sh-HNRNPA2B1-1, sh-HNRNPA2B1-2, sh-HNRNPA2B1-3), METTL3 (sh-METTL3-1, sh-METTL3-2, sh-METTL3-3) or CSNK1D (sh-CSNK1D-1, sh-CSNK1D-2, sh-CSNK1D-3) were synthesized by RiboBio (Guangzhou, China) along with their negative control shRNA (sh-NC). Besides, pcDNA3.1 targeting HNRNPA2B1, CSNK1D, BAMBI and FOXO3, as well as miR-93-5p mimics/inhibitor and miR-25-3p mimics/inhibitor were also synthesized by RiboBio. Cell transfection was implemented using Lipofectamine 2000 (XFSJ16444, GIBCO, USA) for 48 h.

TUNEL assay

Transfected ells were washed twice with PBS and fixed with 4% paraformaldehyde (E672002, Sangon Biotech, Shanghai, China) for 15 min, and then permeabilized in 0.25% Triton X-100 (R00285, Leagene, Beijing, China) for 20 min. TUNEL assays were carried out conforming to the manufacturer's instructions (Roche). Briefly, cells were incubated in terminal deoxynucleotidyl transferase (TdT) reaction cocktail at 37 °C for 45 min, and then treated with Click-iT reaction cocktail. The nucleus was stained with DAPI (D9542, Sigma-Aldrich, St. Louis, MO, USA).

Flow cytometry analysis

After transfection, cells were harvested and then stained with FITC-Annexin V and PI according to the instructions (BD Biosciences, San Jose, CA, USA). The cell apoptosis was analyzed with a flow cytometry (DxFLEX, Thermo Fisher Scientific).

Wound healing assay

Cells were plated into 6-well plates and grown to 90% confluence. A scratch on the surface of cells was made using a plastic tip, and then cells were cultured for another 24 h. Scratch images were acquired using a microscope (Olympus, Tokyo, Japan).

Transwell assay

Cells were placed in the upper chamber of each insert (Corning, Cambridge, USA) containing serum-free medium. Lower chambers were added with medium supplemented with 10% fetal bovine serum (600 μL). After 24 h, cells migrated into the lower surface were stained by 5% crystal violet (V5265, Sigma-Aldrich St., Louis, MO, USA) and observed under an Olympus microscope.

In vivo experiment

PC3 cells stably transfected with sh-HNRNPA2B1 or sh-NC plasmids were subcutaneously injected into the abdomen of male BALB/C nude mice (5–7 weeks; 3 mice per group). Mice were purchased from Shanghai Experimental Animal Research Center. Seven days after injection, the tumor volume was examined every 3 days according to the formula: volume = length × width^2/2. After 28 days, the mice were euthanized through cervical dislocation and tumors were imaged and weighted. The animal studies were approved by the Ethics Committee of Nanjing Medical University.

Immunofluorescence (IF) assay

HNRNPA2B1 antibodies (14813–1-AP, Proteintech, Chicago, IL, USA) were obtained for IF assay. Briefly, cells were fixed by 4% PFA, permeabilized via 0.1% Triton X-100, and cultured with anti-HNRNPA2B1 (1/1000, ab259894, Abcam, Cambridge, MA, USA). After visualization of HNRNPA2B1 through secondary antibodies, cell nuclei underwent counterstaining by utilizing DAPI staining. Images were captured using a fluorescence microscope (XSP-63B, Shanghai Optical Instrument Factory).

Dual-luciferase reporter assay

This assay was carried out using the pmirGLO Dual-Luciferase Vector System (Promega, Madison, WI, USA).

The recombinant pmirGLO + BAMBI-3' UTR, pmirGLO + FOXO3-3' UTR and their corresponding mutant plasmids were established separately following the instructions, which were then transfected into cells with the indicated transfection plasmid using the Lipofectamine 3000 reagent, followed by the detection of the luciferase activities using a dual luciferase reporter assay kit (Promega).

Co-immunoprecipitation (Co-IP) assay and mass spectrometry analysis

Cells were harvested and lysed with IP lysis buffer (P0013, Beyotime, Shanghai, China) on ice, and then centrifuged. The supernatant was incubated with primary antibodies, including anti-HNRNPA2B1 (1/100, ab31645, Abcam) and anti-CSNK1D (1/100, ab236601, Abcam) at 4 °C overnight, and then incubated with protein A/G agarose beads (78610, Thermo Fisher Scientific, Rockford, IL, USA). The next day, the beads were washed five times and then subjected to western blot analysis or mass spectrometry analysis.

Mass spectrometry analysis was carried out by Applied Protein Technology (Shanghai, China) through using 5800 MALDI-TOF/TOF (AB Sciex, USA) for data analyses. For quantitative analysis, a protein must have at minimum one unique peptide match with the MS ratios. Proteins with cut-off value ≥ 3.0 or ≤ 3.0-fold were defined to be up-regulated and down-regulated when p value lower than 0.05. The original data for mass spectrometry analysis are shown in Supplementary file 1.

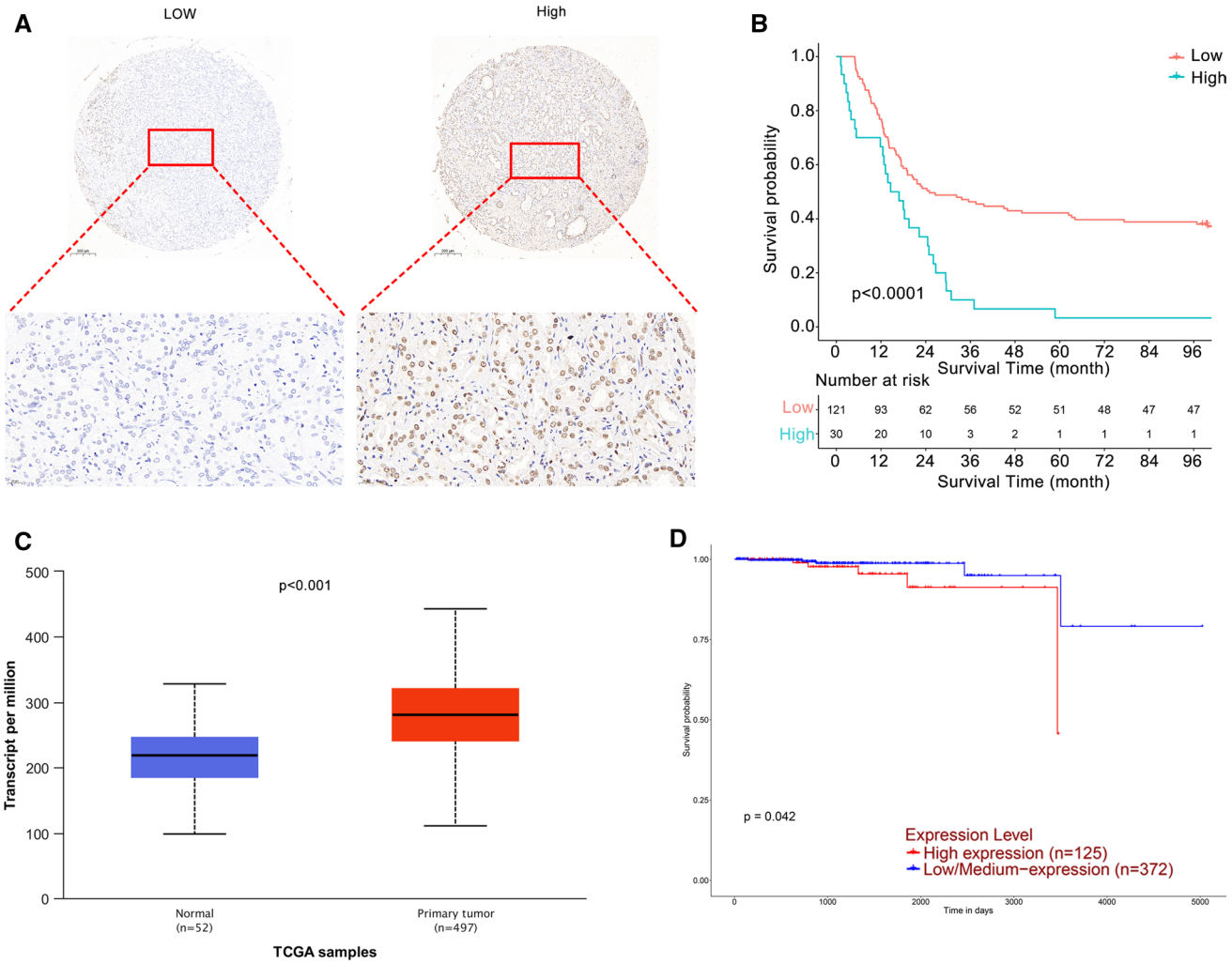

Fig. 1 HNRNPA2B1 expression is up-regulated in PCa tissues and indicated poor survival of PCa patients. **A** Different immunohistochemistry results of HNRNPA2B1 expression in microarray. **B** Kaplan–Meier curves of prostate patients based on HNRNPA2B1 expression levels. Patients with low HNRNPA2B1 expression had obviously longer biochemical recurrence-free survival than those with HNRNPA2B1 expression (log-rank test, $P < 0.0001$). **C** The expression level of HNRNPA2B1 in PCa tissues and normal prostate tissues included TCGA database was identified ($P < 0.001$). D The correlation between HNRNPA2B1 expression and the overall survival rate of PCa patients ($P = 0.042$)

Table 1 Relationship of HNRNPA2B1 expression and clinicopathologic characteristics of prostate patients

Variables	HNRNPA2B1 expression		*P* value
	Low	High	
N	121	30	
Age, year			0.177
< 70	60 (49.59%)	19 (63.33%)	
≥ 70	61 (50.41%)	11 (36.67%)	
PSA, ng/mL			0.453
< 10	27 (22.31%)	5 (16.67%)	
[10–20)	24 (19.83%)	9 (30.00%)	
≥ 20	70 (57.85%)	16 (53.33%)	
Gleason score			0.034
< 7	19 (15.70%)	2 (6.67%)	
= 7	53 (43.80%)	8 (26.67%)	
> 7	49 (40.50%)	20 (66.67%)	
T stage			0.005
T2	80 (66.12%)	11 (36.67%)	
T3	26 (21.49%)	9 (30.00%)	
T4	15 (12.40%)	10 (33.33%)	
N stage			0.004
N0	64 (52.89%)	9 (30.00%)	
N1	17 (14.05%)	12 (40.00%)	
Nx	40 (33.06%)	9 (30.00%)	

Data were *n* (%)

PSA prostate-specific antigen

GST pull-down assay

GST Fusion protein Isotope ([γ-32P] ATP) kinase Labeling Kit (MS11006, GENMED, USA) was performed to purify GST-HNRNPA2B1 or GST proteins following the instructions. The purified proteins were added to cell lysates for rotation. After washing and elution, the proteins were subjected to 10% SDS-PAGE, followed by western blot.

Western blot

Total protein was extracted from cells using RIPA lysis buffer (PROTTOT-1KT, Sigma-Aldrich, USA). Bradford protein concentration determination kit (PC0010, Solarbio, China) was used to measure protein concentration. Extracted proteins were separated by SDS-PAGE (P1200, Solarbio, China) and transferred to PVDF membranes, which were subsequently blocked with a 5% solution of non-fat milk. Membranes were then incubated with primary antibodies, including anti-HNRNPA2B1 (1/1000, ab31645, Abcam), anti-CSNK1D (1/1000, ab236601, Abcam), anti-p21 (1/1000, ab109520, Abcam), anti-p53 (1/10000, ab154036, Abcam), anti-p-SMAD2 (1/1000, ab280888, Abcam), anti-p-SMAD3 (1/1000, ab63403, Abcam), anti-p65 (1/1000, ab32536, Abcam), anti-p50 (1/1000, ab283688, Abcam), anti-FOXO3 (1/2000, ab70315, Abcam), anti-p15 (1/1000, ab53034, Abcam), anti-p-AKT (1/1000, ab38449, Abcam), anti-p-mTOR (1/1000, ab109268, Abcam), anti-p-p38 (1/1000, ab195049, Abcam), anti-p-ERK (1/1000, ab131438, Abcam), anti-p19 (1/1000, ab80, Abcam), and the internal control β-actin (1/1000, ab8226, Abcam). Then, the membranes were washed and incubated with appropriate secondary antibodies (1/2000, ab7063, Abcam). The ECL chemiluminescence system (32134, Pierce Biotechnology, Rockford, IL, USA) was used to detect the signal.

m6A RNA immunoprecipitation (MeRIP) assay

This experiment was performed as per the previous protocol [20]. As guided, Magna ChIP Protein A + G Magnetic Beads (2923270, Millipore, Bedford, MA, USA), anti-m6A polyclonal antibody (ab208577, Abcam) and mouse control IgG (sc-2025, Santa Cruz Biotechnology, Inc., Santa Cruz, CA, USA) were used. The RNA in the immunoprecipitates captured by anti-m6A or IgG was examined by using RT-qPCR.

RNA immunoprecipitation (RIP) assay

RIP assay was conducted using EZMagna RIP kit (Sigma-Aldrich, St. Louis, MO, USA). In brief, cell lysates were mixed with HNRNPA2B1 antibody (14813–1-AP, Proteintech, Rosemont, IL, USA) or the negative control IgG antibody (sc-2025, Santa Cruz Biotechnology, Inc.) at 4℃ overnight, and the RNA products enriched in each group were analyzed via RT-qPCR.

Bioinformatics analysis of RNA-Seq data

The mRNA expression profiles in PC3 cells transfected with miR-93-5p inhibitor/miR-25-3p inhibitor or inhibitor NC were acquired using transcriptome profiling and analyzed using GeneSpring7.0 software (http://www.silicongenetics.com). Genes expression with fold change less than twofold were excluded from further analysis. Then, Kyoto Encyclopedia of Genes and Genomes (KEGG) databases were used for enrichment analysis to ascertain pathways in the downstream of miR-93-5p or miR-25-3p.

RNA pull-down assay

To demonstrate the interaction between miR-93-5p and BAMBI 3'UTR, Biotin-labeled BAMBI 3'UTR (Bio-BAMB-3'UTR), Biotin-labeled BAMBI 3'UTR without complementary base pairing with miR-93-5p (Bio-BAMBI-3'UTR (MUT)) and Biotin-labeled negative control

Table 2 Univariate and multivariate Cox proportional hazards regression model for biochemical recurrence-free survival in patients with prostate cancer

	Univariate		Multivariate	
	HR (95% CI)	*P* value	HR (95% CI)	*P* value
Age, year		0357		
< 70	1		1	
≥ 70	0.839 (0.578–1.219)			
PSA, ng/mL		0.014		0.276
< 10	1		1	
[10–20)	1.709 (0.909–3.212)	0.096	1.662 (0.872–3.167)	0.122
≥ 20	2.215 (1.294–3.791)	0.004	1.481 (0.820–2.677)	0.193
Gleason score		< 0.001		0.010
< 7	1		1	
= 7	1.837 (0.888–3.802)	0.101	1.579 (0.733–3.403)	0.244
> 7	4.388 (2.159–8.918)	< 0.001	2.908 (1.265–6.688)	0.012
T stage		< 0.001		0.005
T2	1		1	
T3	2.114 (1.353–3.302)	0.001	1.423 (0.858–2.361)	0.172
T4	4.549 (2.725–7.592)	< 0.001	2.831 (1.502–5.335)	0.001
N stage		< 0.001		0.001
N0	1		1	
N1	3.227 (1.977–5.267)	< 0.001	1.612 (0.912–2.850)	0.100
Nx	2.049 (1.330–3.157)	0.001	2.360 (1.516–3.673)	< 0.001
HNRNPA2B1		< 0.001		0.040
Low	1		1	
High	2.537 (1.646–3.910)	< 0.001	1.623 (1.022–2.578)	0.040

HR hazard ratio, *CI* confidence interval, *PSA* prostate-specific antigen

sequence (Bio-NC) were synthesized by Ribobio. Similarly, Bio-FOXO3-3'UTR, Bio-FOXO3-3'UTR (MUT) and Bio-NC were synthesized. The above biotin-labeled probes were incubated with cell lysates, followed by adding Streptavidin M280 beads (Thermo Fisher Scientific, Waltham, MA, USA). Then, RNA–protein mixtures were eluted and subjected to RT-qPCR to analyze the enrichment of miR-93-5p or miR-25-3p in different groups.

Statistical analysis

All experimental data were presented as the mean ± standard deviation (SD) of three or more repeated experiments using GraphPad PRISM 6 (GraphPad, San Diego, CA, USA). SPSS v22.0 (SPSS, USA) was used for statistical analysis. Differences between two groups or among more than two groups were analyzed by Student's *t* test or one-way ANOVA. Differences were considered to be significant when $P < 0.05$.

Results

HNRNPA2B1 expression is up-regulated in PCa tissues and indicated poor survival of PCa patients

A total of 151 patients were continuedly followed up in this study. The last follow-up time of the study was February 12, 2022, and the median follow-up time was 21.67 [interquartile range (IQR = 11.18–105.50)] months. IHC was performed to assess the expression of HNRNPA2B1 in tumor tissues obtained from PCa patients (Fig. 1A). All patients were divided into two groups, including low HNRNPA2B1 expression group ($n = 121$) and high HNRNPA2B1 expression group ($n = 30$), according to IHC results. Table 1 revealed the close correlation between higher HNRNPA2B1 expression and higher Gleason score ($P = 0.034$), T stage ($P = 0.005$) and N stage ($P = 0.004$). Kaplan–Meier analysis showed that PCa patients with high HNRNPA2B1 expression had significantly worse bRFS than those with low HNRNPA2B1 expression ($P < 0.0001$) (Fig. 1B). Moreover, multivariate Cox regression analyses (Table 2) indicated that Gleason score ($P = 0.010$), T stage ($P = 0.005$), N stage ($P = 0.001$) and HNRNPA2B1 expression ($P = 0.040$) were intendent risk factors of bRFS in PCa patients. We also analyzed data in TCGA database and confirmed that

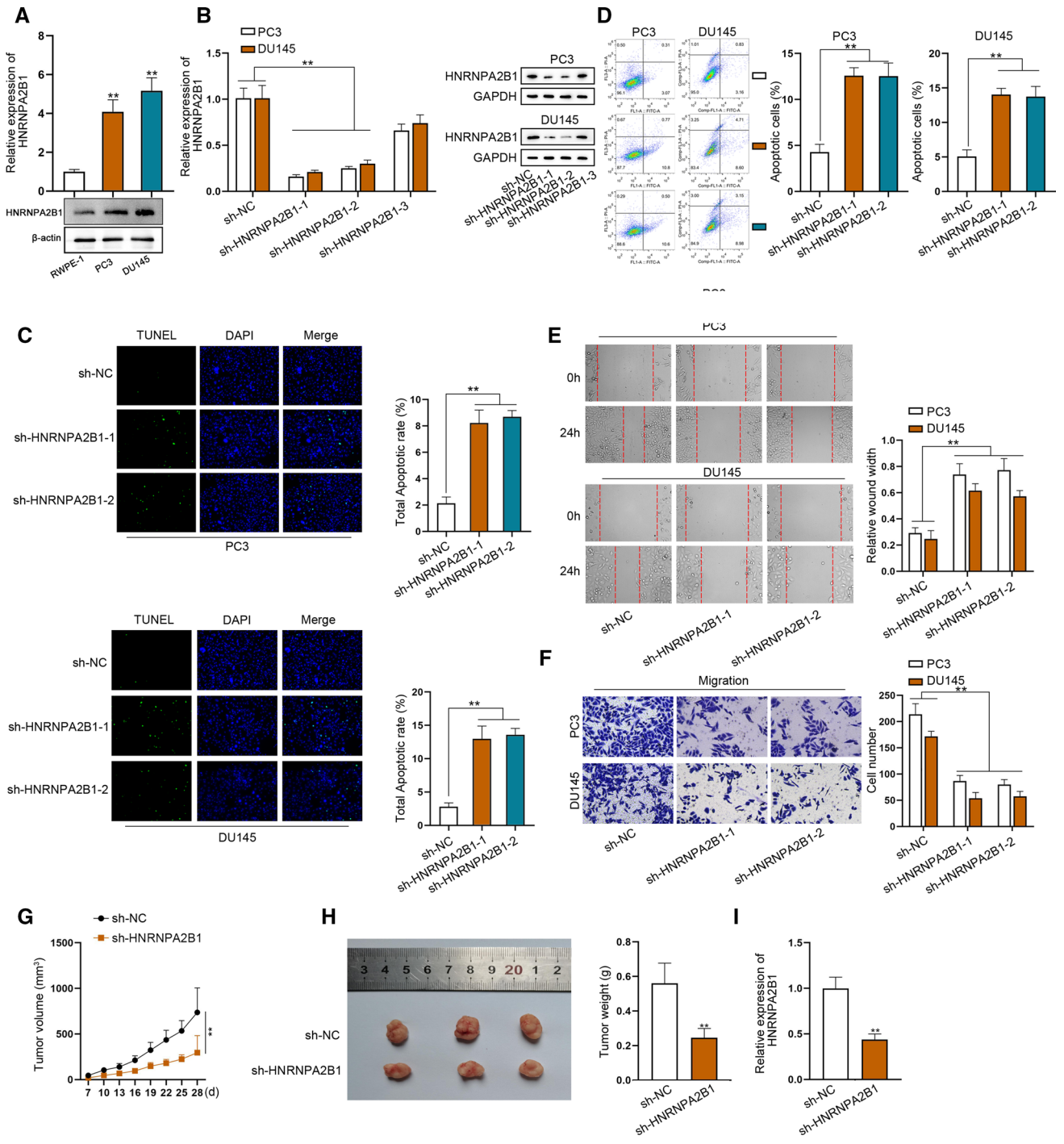

Fig. 2 HNRNPA2B1 promotes the malignant processes of PCa cells both in vitro and in vivo. **A** RT-qPCR detected HNRNPA2B1 expression in PCa cells. **B** Inhibition efficiency of HNRNPA2B1 was detected by RT-qPCR and western blot. **C**, **D** TUNEL assay and flow cytometry analysis detected PCa cell apoptosis after HNRNPA2B1 silence. **E**, **F** Wound healing and transwell assays detected PCa cell migration after HNRNPA2B1 silence. **G**, **H** Tumor volume and tumor weight were measured in groups with or without HNRNPA2B1 silence. **I** HNRNPA2B1 expression was detected by RT-qPCR in tumors from indicated groups. $^{**}P < 0.01$

HNRNPA2B1 expression was significantly higher in PCa tissues than that in normal prostate tissues (Fig. 1C). Meanwhile, higher HNRNPA2B1 expression indicated the low overall survival rate of PCa patients, as analyzed using Kaplan–Meier method (Fig. 1D). Therefore, we confirmed the ectopic expression of HNRNPA2B1 in PCa samples and its correlation with patients' prognosis.

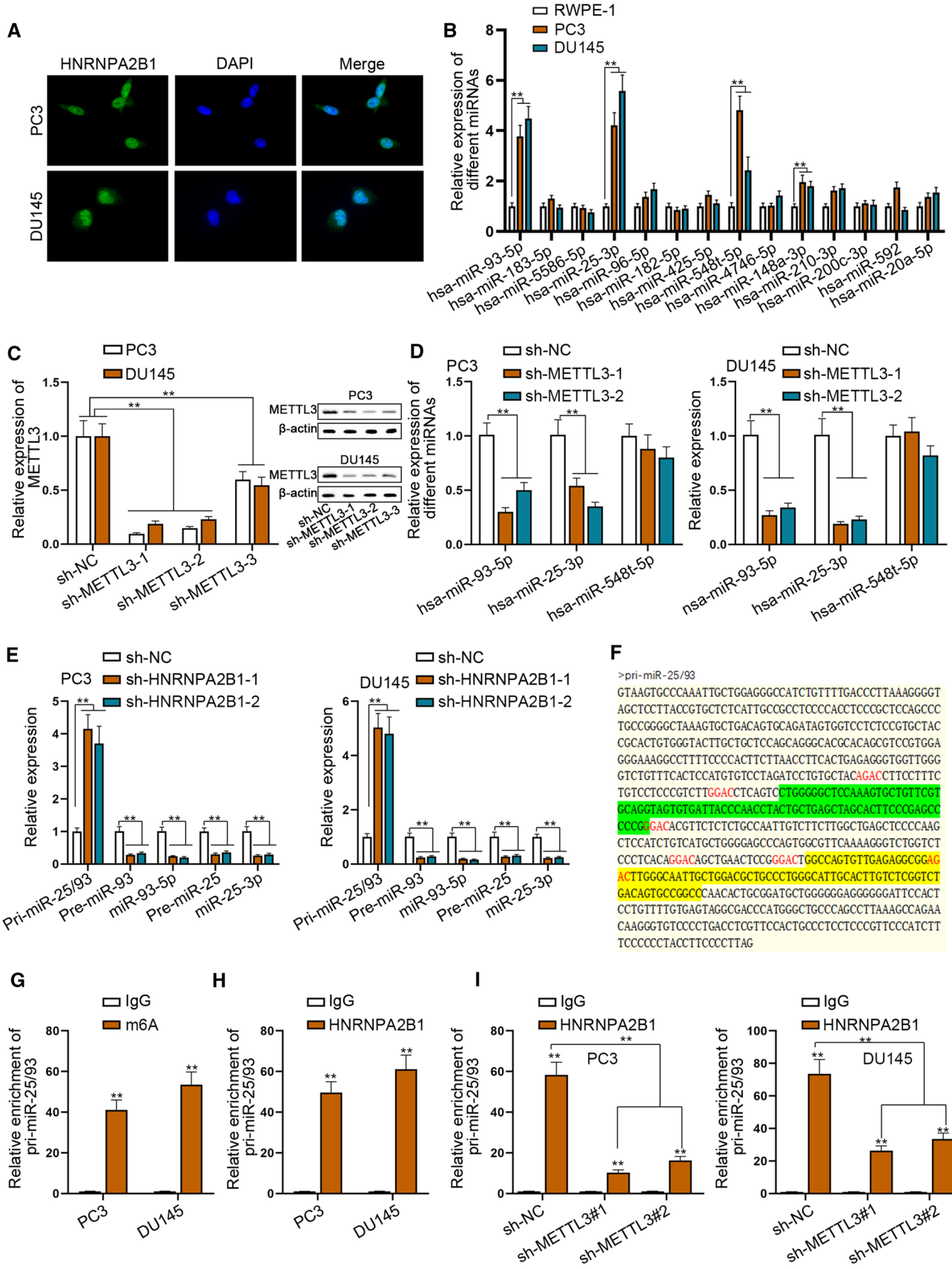
A
HNRNPA2B1
DAPI
Merge
PC3
DU145
B
RWPE-1
PC3
DU145
Relative expression of different miRNAs
hsa-miR-93-5p
hsa-miR-183-5p
hsa-miR-5586-5p
hsa-miR-25-3p
hsa-miR-96-5p
hsa-miR-182-5p
hsa-miR-425-5p
hsa-miR-548t-5p
hsa-miR-4746-5p
hsa-miR-148a-3p
hsa-miR-210-3p
hsa-miR-200c-3p
hsa-miR-592
hsa-miR-20a-5p
C
PC3
DU145
Relative expression of METTL3
sh-NC
sh-METTL3-1
sh-METTL3-2
sh-METTL3-3
METTL3
β-actin
D
sh-NC
sh-METTL3-1
sh-METTL3-2
Relative expression of different miRNAs
Relative expression
hsa-miR-93-5p
hsa-miR-25-3p
hsa-miR-548t-5p
E
sh-NC
sh-HNRNPA2B1-1
sh-HNRNPA2B1-2
Relative expression
Pri-miR-25/93
Pre-miR-93
miR-93-5p
Pre-miR-25
miR-25-3p
F
>pri-miR-25/93
GTAAGTGCCCAAATTGCTGGAGGGCCATCTGTTTTGACCCTTAAAGGGGT
AGCTCCTTACCGTGCTCTCATTGCCGCCTCCCCACCTCCCGCTCCAGCCC
TGCCGGGGCTAAAGTGCTGACAGTGCAGATAGTGGTCCTCTCCGTGCTAC
CGCACTGTGGGTACTTGCTGCTCCAGCAGGGCACGCACAGCGTCCGTGGA
GGGAAAGGCCTTTTCCCCACTTCTTAACCTTCACTGAGAGGGTGGTTGGG
GTCTGTTTCACTCCATGTGTCCTAGATCCTGTGCTACAGACCTTCCTTTC
TGTCCTCCCGTCTTGGACCTCAGTCCTGGGGGCTCCAAAGTGCTGTTCGT
GCAGGTAGTGTGATTACCCAACCTACTGCTGAGCTAGCACTTCCCGAGCC
CCCGGGACACGTTCTCTCTGCCAATTGTCTTCTTGGCTGAGCTCCCCAAG
CTCCATCTGTCATGCTGGGGAGCCCAGTGGCGTTCAAAAGGGTCTGGTCT
CCCTCACAGGACAGCTGAACTCCGGGACTGGCCAGTGTTGAGAGGCGGAG
ACTTGGGCAATTGCTGGACGCTGCCCTGGGCATTGCACTTGTCTCGGTCT
GACAGTGCCGGCCCAACACTGCGGATGCTGGGGGGAGGGGGGATTCCACT
CCTGTTTTGTGAGTAGGCGACCCATGGGCTGCCCAGCCTTAAAGCCAGAA
CAAGGGTGTCCCCTGACCTCGTTCCACTGCCCTCCTCCCGTTCCCATCTT
TCCCCCCTACCTTCCCCTTAG
G
IgG
m6A
Relative enrichment of pri-miR-25/93
PC3
DU145
H
IgG
HNRNPA2B1
I
IgG
HNRNPA2B1
PC3
DU145
sh-NC
sh-METTL3#1
sh-METTL3#2

◂**Fig. 3** HNRNPA2B1 induces miR-25-3p/miR-93-5p maturation by recognizing the m^{6}A site. **A** IF assay detected HNRNPA2B1 location in PCa cells. **B** RT-qPCR detected the expression of HNRNPA2B1-related miRNAs suggested by TCGA in PCa cells. **C** Inhibition efficiency of METTL3 was detected by RT-qPCR and western blot. **D** Expression of three miRNAs was detected by RT-qPCR after METTL3 silence. **E** RT-qPCR detected the expression of pri-miR-25/93, pre-miR-93, pre-miR-25 and mature miR-93-5p/miR-25-3p after HNRNPA2B1 silence. **F** RGAC site in pri-miR-25/93 were marked in red. The sequences of pre-miR-93 and pre-miR-25 highlighted in green or yellow background, respectively. **G** meRIP assay validated the existence of m6A modification in pri-miR-25/93 in PC3 and DU145 cells. **H** RIP experiment detected the recognition of pri-miR-25/93 by HNRNPA2B1 in PCa cells. **I** RIP assay analyzed the impact of METTL3 interference on the binding of HNRNPA2B1 to pri-miR-25/93. $^{**}P < 0.01$

HNRNPA2B1 promotes the malignant processes of PCa cells both in vitro and in vivo

To clarify the specific role of HNRNPA2B1 in PCa progression, we continued to perform functional assays in PCa cells. Before that, we applied RT-qPCR and western blot to detect the expression pattern of HNRNPA2B1 in PCa cells (PC3 and DU145) and human normal prostate epithelial cell (RWPE-1). As revealed in Fig. 2A, HNRNPA2B1 showed a higher expression level in PCa cells compared to RWPE-1 cells. Subsequently, HNRNPA2B1 were effectively silenced by sh-HNRNPA2B1#1/2 in PC3 and DU145 cells, as demonstrated by RT-qPCR and western blot (Fig. 2B). According to the results of TUNEL assay and flow cytometry analysis, inhibiting HNRNPA2B1 expression apparently elevated apoptosis rate of PCa cells (Fig. 2C, D). Through wound healing assay and Transwell assay, we discovered that HNRNPA2B1 depletion obviously restrained PCa cell migration (Fig. 2E, F). In vivo animal study was conducted to further confirm the impact of HNRNPA2B1 on PCa cell functions. The results showed that the tumor growth rate in sh-HNRNPA2B1 group was much slower than that in the control group (Fig. 2G). After 28 days, the mice were killed and the tumors were obtained and measured. We observed that the size and weight of tumors in the sh-HNRNPA2B1 group were both smaller than those in the control group (Fig. 2H). Similarly, the expression level of HNRNPA2B1 in sh-HNRNPA2B1 group was significantly lower than those in control group (Fig. 2I). These data proved the tumor-promoting role of HNRNPA2B1 in PCa.

HNRNPA2B1 induces miR-25-3p/miR-93-5p maturation by recognizing the m^{6}A site

As reported previously, HNRNPA2B1 is capable of regulating the processing of primary miRNA transcripts (pri-miRNAs) in m^{6}A-dependent manner [6]. Through IF assay, we observed that HNRNPA2B1 was mainly located in the nucleus of PCa cells (Fig. 3A), suggesting the potential of HNRNPA2B1 contribute to the processing of pri-miRNAs into precursor miRNAs (pre-miRNAs). Through analyzing miRNA isoform expression profiling data in TCGA-PRAD, we found 78 miRNAs up-regulated (logFC > 1, adjusted $P < 0.05$) in PRAD cancerous samples, wherein 14 of them had positive expression correlation with HNRNPA2B1 (Pearson's rho > 0.2, $P < 0.05$), including hsa-miR-93-5p, hsa-miR-183-5p, hsa-miR-5586-5p, hsa-miR-25-3p, hsa-miR-96-5p, hsa-miR-182-5p, hsa-miR-425-5p, hsa-miR-548t-5p, hsa-miR-4746-5p, hsa-miR-148a-3p, hsa-miR-210-3p, hsa-miR-200c-3p, hsa-miR-592 and hsa-miR-20a-5p. Thus, we chose these 14 miRNAs for further RT-qPCR analysis. It was found that only hsa-miR-93-5p, hsa-miR-25-3p and hsa-miR-548t-5p were significantly up-regulated in PCa cells relative to RWPE-1 cells (Fig. 3B). HNRNPA2B1 is a reader of m^{6}A site, and its function is based on m^{6}A site. Therefore, we then analyzed which of these 3 candidate miRNAs could be affected by methyltransferase METTL3. We silenced METTL3 expression in PCa cells, and selected sh-METTL3#1/2 for subsequent assays due to their relative higher interference efficiency (Fig. 3C). Results manifested that only the expression levels of hsa-miR-93-5p and hsa-miR-25-3p were markedly decreased after METTL3 interference in both PC3 and DU145 cells (Fig. 3D). According to the searching result of UCSC (http://genome.ucsc.edu/), we found that both MIR25 and MIR93 were located within the intron 12 of MCM7 gene (Figure S1A), hence we named the common primary miRNA of miR-25-3p and miR-93-5p as pri-miR-25/93. Next, we investigated whether HNRNPA2B1 affected their maturation. As revealed in Fig. 3E, the level of pri-miR-25/93 was significantly increased, while that of pre-miR-93, mature miR-93-5p, pre-miR-25 and mature miR-25-3p were decreased after HNRNPA2B1 silence. Further, we discovered several m6A modification sites (consensus motif RGAC sites, R represents purine, marked in red) in 50 nt upstream of pre-miR-25 and pre-miR-93 (Fig. 3F). Through meRIP assay, we verified that pri-miR-25/93 could be equipped with m6A modification in both PC3 and DU145 cells (Fig. 3G). Besides, the recognition of pri-miR-25/93 by HNRNPA2B1 was also validated by RIP assay, as shown in Fig. 3H. More importantly, silencing of METTL3 impaired the binding of HNRNPA2B1 to pri-miR-25/93 (Fig. 3I). Based on the above results, we deduced that HNRNPA2B1 facilitates the maturation of miR-25-3p/93-5p in a m6A-dependent manner.

CSNK1D mediates HNRNPA2B1 phosphorylation to stabilize HNRNPA2B1 protein

Subsequently, we probed into the upstream mechanism of HNRNPA2B1 in PCa. Through IP and mass spectrometry

analysis, we found that that HNRNPA2B1 may interact with a casein kinase CSNK1D (Fig. 4A). Co-IP assay and western blot analysis further proved the interaction between CSNK1D and HNRNPA2B1 was proved (Fig. 4B). CSNK1D is known as a phosphorylation regulator, thus we further explored whether CSNK1D could mediate the of HNRNPA2B1. To predict the phosphorylation sites of HNRNPA2B1 acted by CSNK1D, different HNRNPA2B1 fragments with GST-labeled overexpression vectors were inserted into PC3 cells to perform GST pull-down assay. We found that the phosphorylation sites of HNRNPA2B1 acted by CSNK1D were between aa20-39 in PC3 cells (Fig. 4C). The results predicted from NetPhos (http://www.cbs.dtu.dk/services/NetPhos/) website showed that four phosphorylation sites including T20, T21, S24 and T36 of HNRNPA2B1 within this region (Fig. 4D). Further, we knocked down CSNK1D expression in PC3 cells (Fig. 4E), and found that down-regulation of CSNK1D reduced the phosphorylation of HNRNPA2B1 at threonine site, but not serine site. Meanwhile, the total protein level of HNRNPA2B1 was also decreased by CSNK1D knockdown (Fig. 4F). These data showed that CSNK1D potentially phosphorylated HNRNPA2B1 at T20, T21 or T36. We continued to construct the overexpressed stable cell line PC3-HNRNPA2B1^{T20M}, PC3-HNRNPA2B1T^{21M}and PC3-HNRNPA2B1^{T36M} and used western blot to detect the corresponding protein content. The results showed that loss of CSNK1D still decreased phosphorylation of HNRNPA2B1 after T21 or T36 mutation, while had no impact on the phosphorylation of HNRNPA2B1 with T20 mutation (Fig. 4G), proving that CSNK1D could phosphorylate HNRNPA2B1 protein at T20 site. Besides, in vitro phosphorylation experiment showed that CSNK1D phosphorylated wild-type HNRNPA2B1, while did not influence the phosphorylation of HNRNPA2B1-T20M mutant protein (Fig. 4H), which further proved that T20 was the site where CSNK1D phosphorylated HNRNPA2B1. Given that CSNK1D could affect the level of HNRNPA2B1 total protein, we guessed that the phosphorylation of HNRNPA2B1 mediated by CSNK1D might influence its protein stability. After overexpressing CSNK1D in PC3 cells (Fig. 4I), we found the degradation of

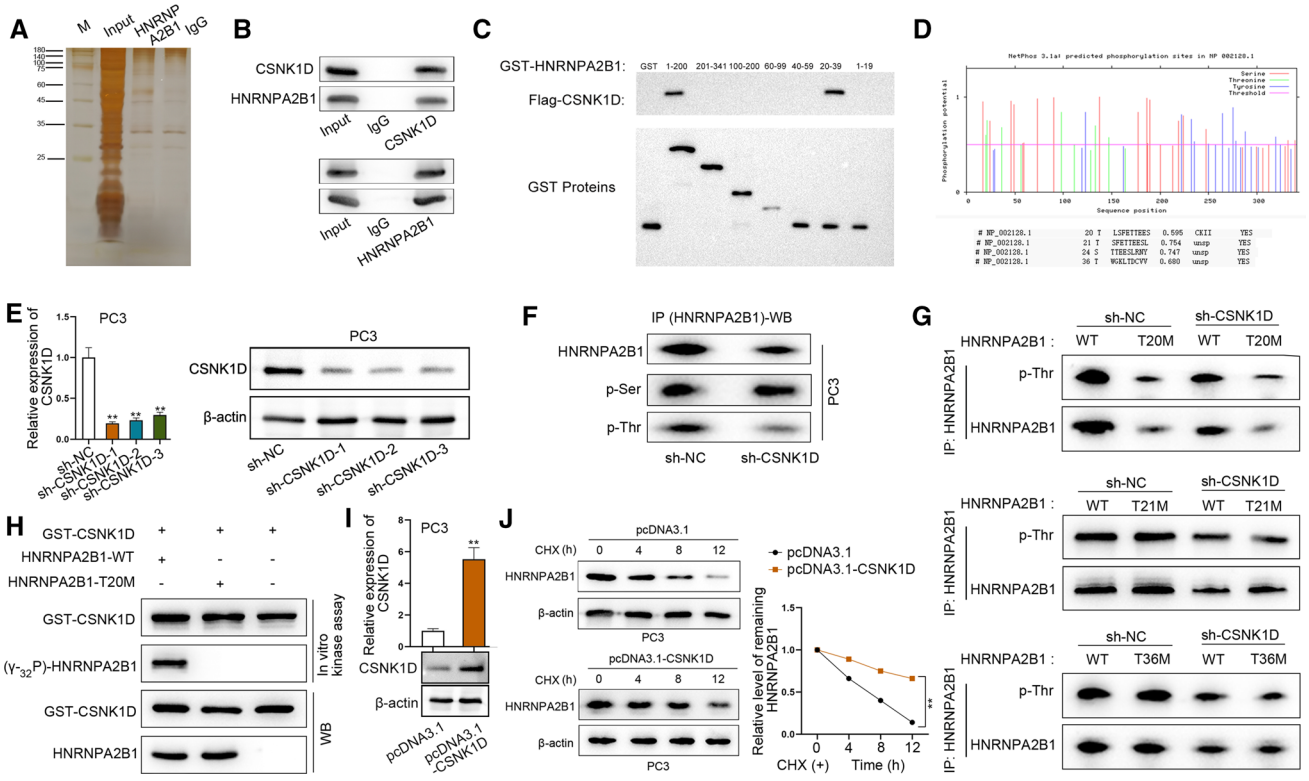

Fig. 4 CSNK1D mediates HNRNPA2B1 phosphorylation and stabilizes HNRNPA2B1 protein. **A** HNRNPA2B1-IP plus mass spectrometry analyzed the interactors of HNRNPA2B1 in PC3 cells. **B** Co-IP assay detected the interaction between CSNK1D and HNRNPA2B1. **C** GST pull-down assay detected the binding of Flag-CSNK1D to different fragments of HNRNPA2B1. **D** NetPhos website predicted the phosphorylation site of HNRNPA2B1. **E** Inhibition efficiency of CSNK1D was tested by RT-qPCR and western blot. **F** IP-WB assay detected the effects of CSNK1D inhibition on HNRNPA2B1 phosphorylation. **G** IP-WB detected the effects of CSNK1D inhibition on the phosphorylation of corresponding HNRNPA2B1 proteins with indicated site mutation. **H** In vitro kinase experiment analyzed the role of CSNK1D on HNRNPA2B1-T20 phosphorylation. **I** Overexpression efficiency of CSNK1D was detected by RT-qPCR. **J** Western blot analyzed the level of HNRNPA2B1 protein after CSNK1D overexpression in the presence of CHX. $^{**}P < 0.01$

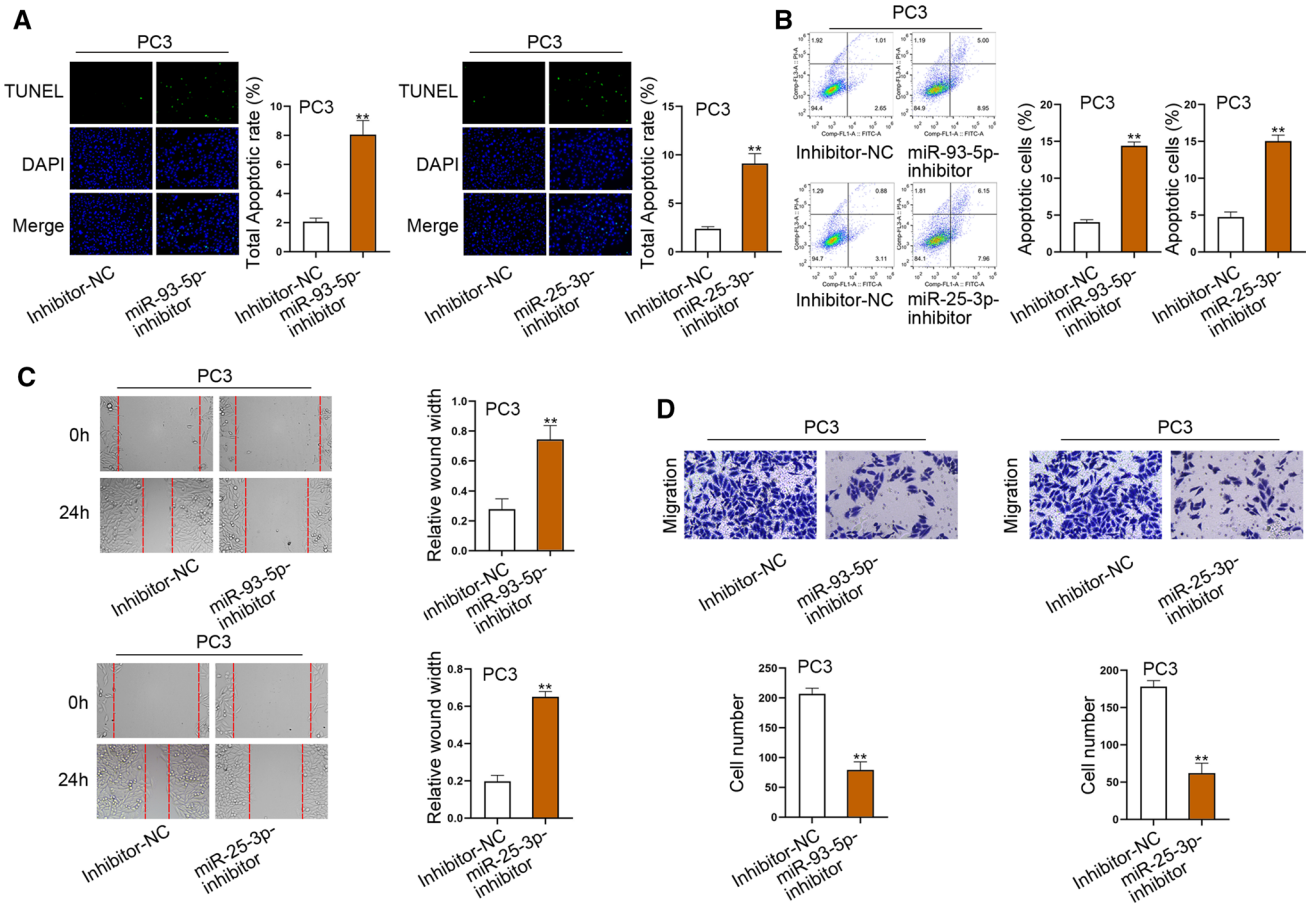

Fig. 5 MiR-93-5p and miR-25-3p regulate PCa cell apoptosis and migration. **A**, **B** TUNEL assay and flow cytometry analysis detected PC3 cell apoptosis after miR-93-5p or miR-25-3p inhibition. **C**, **D** Wound healing and transwell assays detected PC3 cell migration after miR-93-5p or miR-25-3p inhibition. $^{**}P < 0.01$

HNRNPA2B1 under CHX treatment was retarded (Fig. 4J), indicating that the presence of CSNK1D enhances the stability of HNRNPA2B1 protein.

MiR-93-5p and miR-25-3p regulate PCa cell apoptosis and migration

The impacts of miR-93-5p and miR-25-3p on the functions of PCa cells were probed. Through TUNEL assay and flow cytometry analysis, we found that silencing of miR-93-5p or miR-25-3p could accelerate PCa cell apoptosis (Fig. 5A, B). Moreover, we proved that inhibiting expression of miR-93-5p or miR-25-3p hindered PCa cell migration (Fig. 5C, D).

MiR-93-5p activates TGF-β pathway by inhibiting BAMBI expression

MiRNAs regulate gene expression by promoting mRNA degradation or inhibiting its translation [21]. Therefore, we explored the downstream mRNAs and pathways of miR-93-5p and miR-25-3p. Through transcriptome analysis of possible downstream pathways underlying miR-93-5p, pathways with p value ≤ 0.20 and widely studied in cancer were selected as research objects. Hence, p53 signaling pathway, TGF-beta signaling pathway and NF-kappa B signaling pathway were selected (Table S1). Western blot analysis further detected the levels of key proteins involved in above three pathways. It manifested that the levels of p-Smad2 and p-Smad3 were aberrantly decreased after interference with miR-93-5p, while the expression levels of p53, p21, p65 and p50 remained unchanged (Fig. 6A), suggesting that miR-93-5p could affect the TGF-β pathway. Besides, we found that the levels of

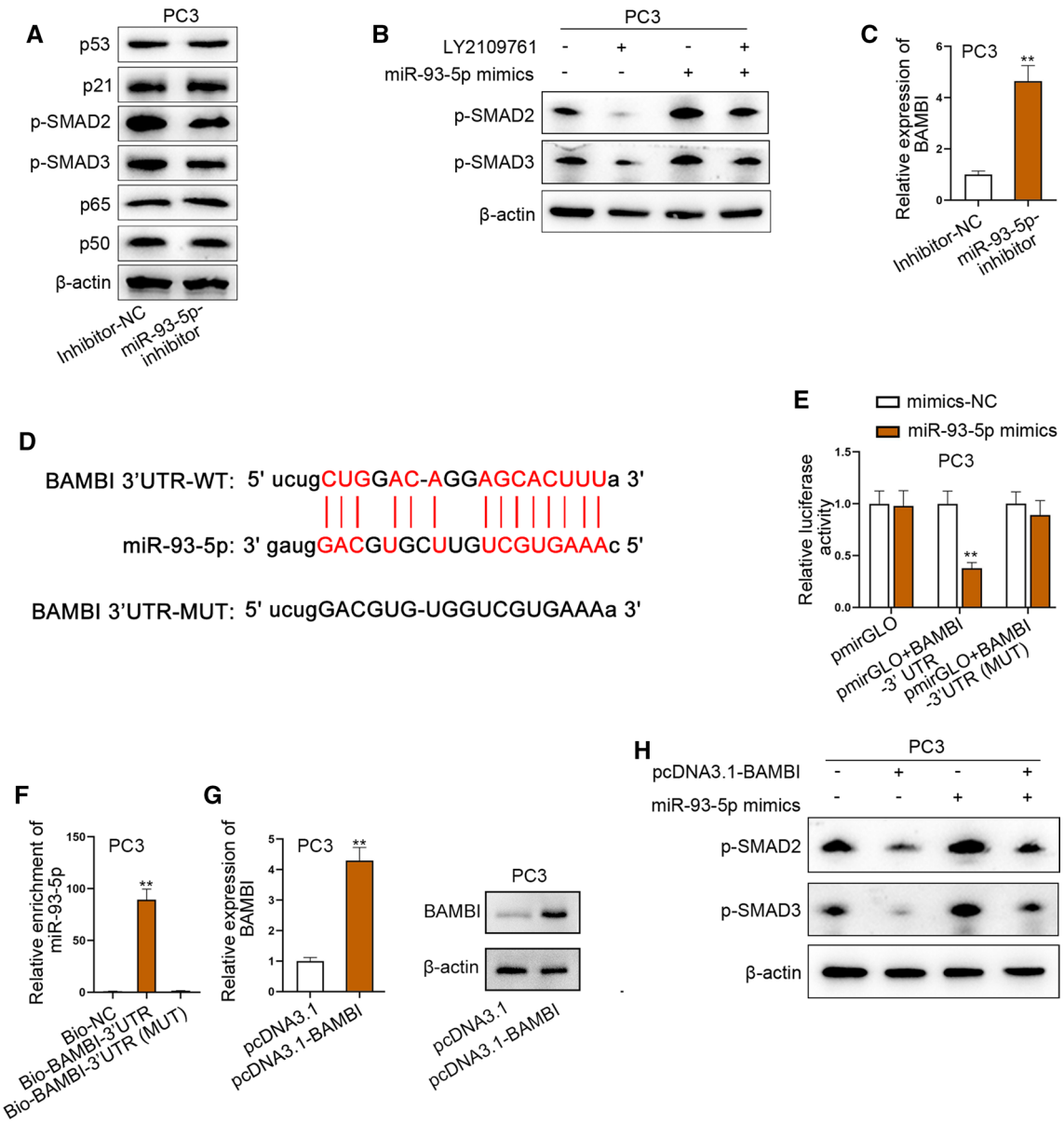

Fig. 6 MiR-93-5p activates TGF-β pathway by inhibiting BAMBI expression. **A** Western blot analyzed the influence of miR-93-5p on the levels of key proteins involved in p53, TGF-β and NF-κB pathways. **B** Western blot analyzed the levels of p-SMAD2 and p-SMAD3 in PC3 cells after miR-93-5p overexpression or LY2109761 addition. **C** RT-qPCR detected BAMBI expression after miR-93-5p inhibition. **D** The binding sites between miR-93-5p and BAMBI 3'UTR. **E** The luciferase activity of pmirGLO + BAMBI-3' UTR and pmirGLO + BAMBI-3'UTR (MUT) was assessed after miR-93-5p overexpression. **F** RNA pull-down assay detected the binding between BAMBI and miR-93-5p. **G** Overexpression efficiency of BAMBI was detected by RT-qPCR and western blot. **H** Western blot analyzed the levels of p-SMAD2 and p-SMAD3 in PC3 cells after miR-25-3p overexpression or BAMBI overexpression. $^{**}P < 0.01$

p-Smad2 and p-Smad3 were increased when miR-93-5p was up-regulated, but this effect was reversed after addition of LY2109761, TGF-β pathway inhibitor (Fig. 6B). To explore the approach through which miR-93-5p affects TGF-β pathway, we searched ENCORI (http://starbase.sysu.edu.cn) website for potential miR-93-5p target which related to TGF-β pathway. Fortunately, ENCORI predicted that miR-93-5p bound to the TGF-β pathway inhibitor BAMBI (Table S2). Also, the expression of BAMBI was promoted when miR-93-5p was inhibited (Fig. 6C). The binding sites between miR-93-5p and BAMBI 3'UTR were obtained and listed in Fig. 6D. At the same time, the luciferase activity of pmirGLO + BAMBI-3' UTR was lessened when miR-93-5p was overexpressed (Fig. 6E), suggesting

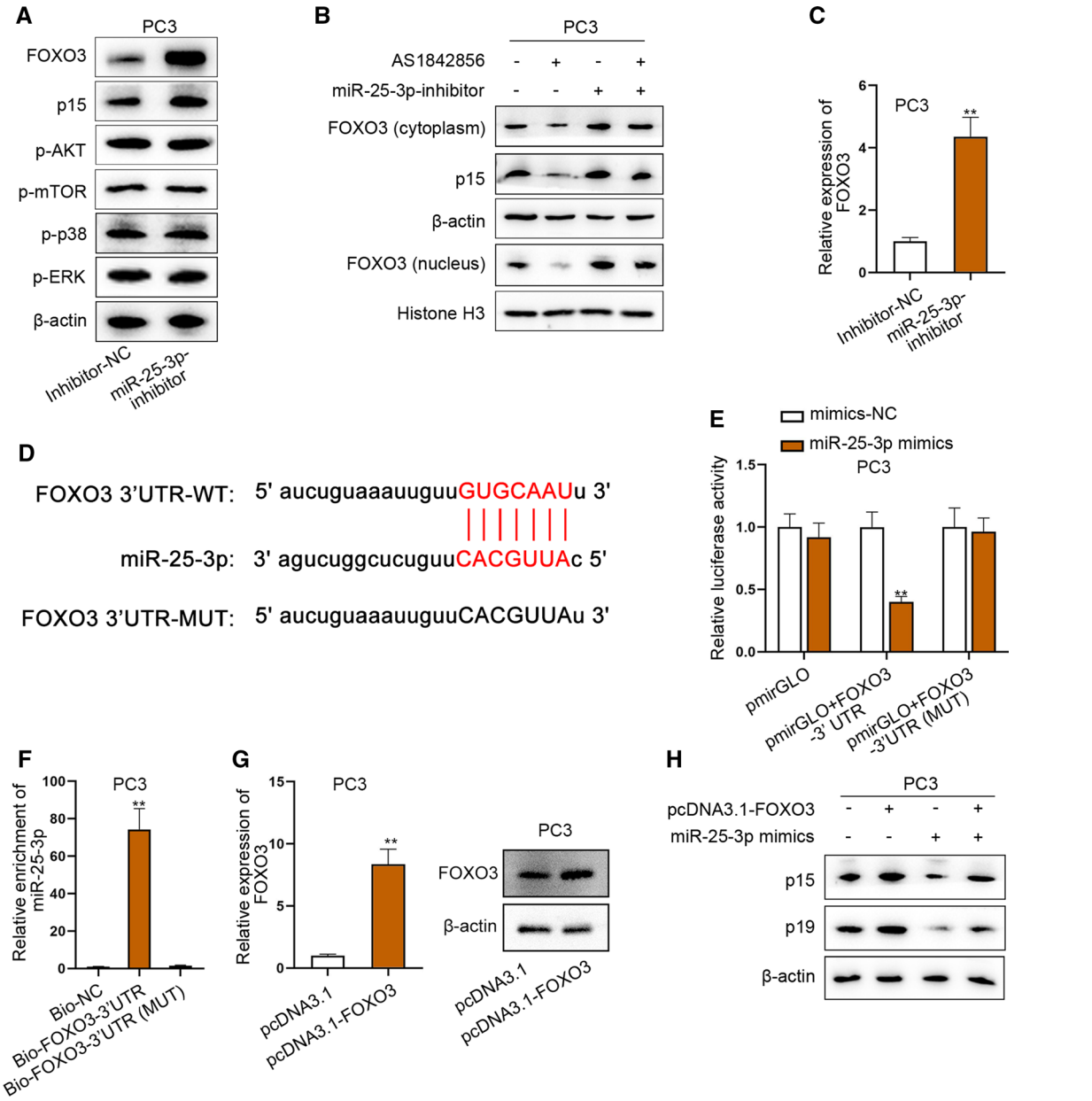

Fig. 7 MiR-25-3p inhibits FOXO pathway by targeting FOXO3. **A** Western blot analyzed the levels of key proteins in FOXO, PI3K/Akt and MAPK pathways after miR-25-3p inhibition. **B** Western blot analyzed the levels of p15, cytoplasmic and nuclear FOXO3 in PC3 cells after miR-25-3p inhibition or AS1842856 addition. **C** RT-qPCR detected FOXO3 expression after miR-25-3p inhibition. **D** The binding sites between miR-25-5p and BAMBI 3'UTR. **E** The luciferase activity of pmirGLO + FOXO3-3' UTR and pmirGLO + FOXO3-3'UTR (MUT) was assessed after miR-25-3p overexpression. **F** RNA pull-down assay detected the binding between FOXO3 and miR-25-3p. **G** Overexpression efficiency of FOXO3 was detected by RT-qPCR and western blot. **H** Western blot analyzed the levels of p15 and p19 in PC3 cells after miR-25-3p upregulation or FOXO3 overexpression. $^{**}P < 0.01$

that miR-93-5p could act on BAMBI 3'UTR. Moreover, we found that miR-93-5p could bind to BAMBI-3' UTR through RNA pull-down assay (Fig. 6F). Next, we overexpressed BAMBI in PCa cells (Fig. 6G), and found that the increased levels of p-Smad2 and p-Smad3 caused by miR-93-5p overexpression could be offset after co-transfection of pcDNA3.1-BAMBI (Fig. 6H). In summary, miR-93-5p can activate TGF-β pathway by inhibiting BAMBI expression.

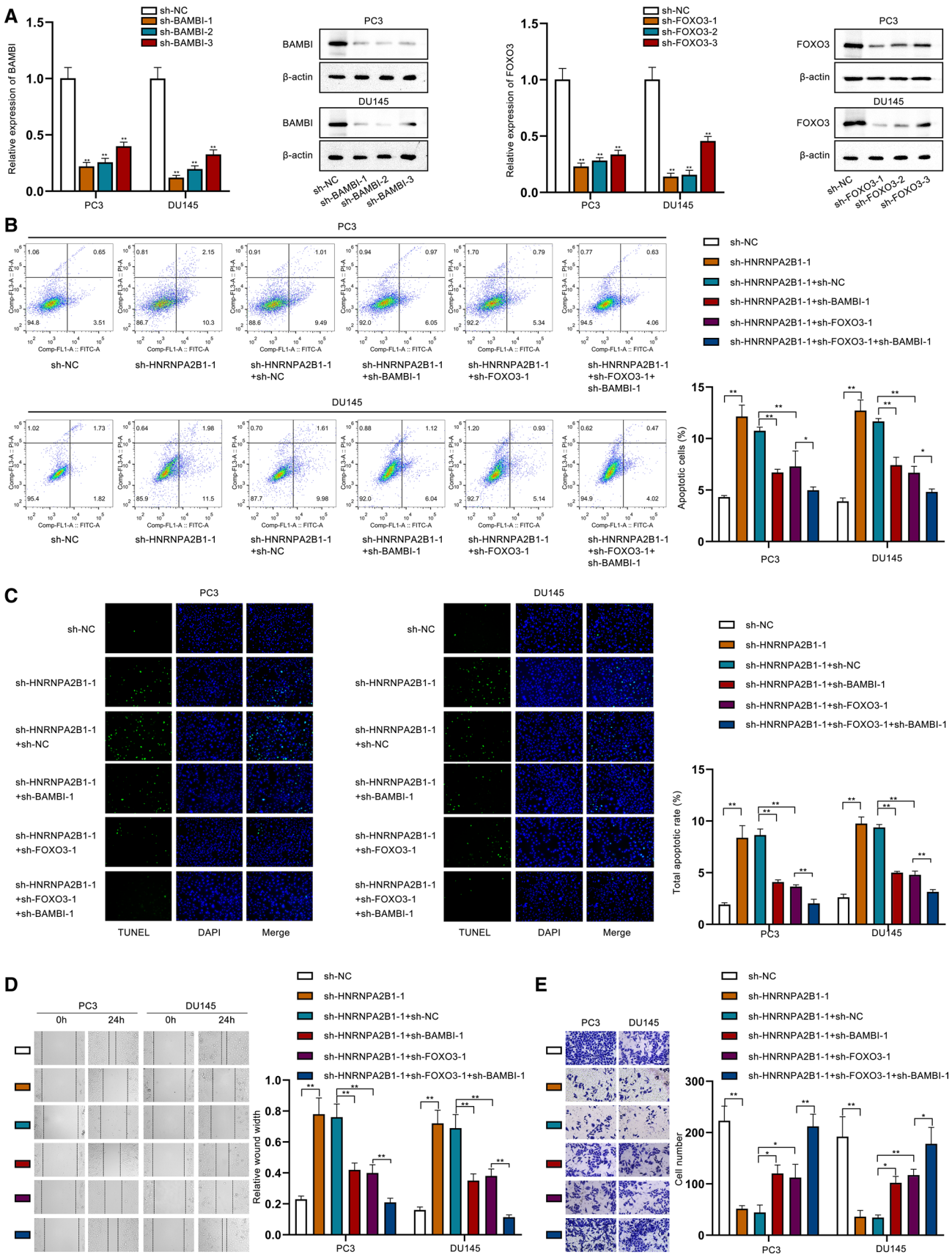
A
sh-NC
sh-BAMBI-1
sh-BAMBI-2
sh-BAMBI-3
Relative expression of BAMBI
PC3
DU145
BAMBI
β-actin
sh-NC
sh-BAMBI-1
sh-BAMBI-2
sh-BAMBI-3
sh-FOXO3-1
sh-FOXO3-2
sh-FOXO3-3
Relative expression of FOXO3
FOXO3
sh-FOXO3-1
sh-FOXO3-2
sh-FOXO3-3
B
PC3
DU145
sh-NC
sh-HNRNPA2B1-1
sh-HNRNPA2B1-1+sh-NC
sh-HNRNPA2B1-1+sh-BAMBI-1
sh-HNRNPA2B1-1+sh-FOXO3-1
sh-HNRNPA2B1-1+sh-FOXO3-1+sh-BAMBI-1
Apoptotic cells (%)
C
TUNEL
DAPI
Merge
Total apoptotic rate (%)
D
0h
24h
Relative wound width
E
Cell number

◂**Fig. 8** BAMBI and FOXO3 jointly involves in HNRNPA2B1-mediated PCa cell apoptosis and migration. **A** BAMBI and FOXO3 was separately silenced in two PCa cells, as detected by RT-qPCR and western blot. **B**, **C** Flow cytometry and TUNEL assay detected the effects of silencing of BAMBI or FOXO3 on the apoptosis of PCa cells with HNRNPA2B1 knockdown. **D**, **E** Wound healing assay and transwell assay detected the effects of silencing of BAMBI or FOXO3 on the migration of PCa cells with HNRNPA2B1 knockdown. $^{*}P<0.05$, $^{**}P<0.01$

MiR-25-3p inactivates the FOXO pathway by targeting FOXO3

Similarly, using transcriptome analysis of possible downstream pathways underlying miR-25-3p, pathways with p value ≤ 0.20 and widely studied in cancer were selected as research objects. In this regard, we focused on FOXO signaling pathway, PI3K-Akt signaling pathway and MAPK signaling pathway (Table S3). Western blot analysis further indicated that the levels of p15 and FOXO3 were enhanced after miR-25-3p inhibition, while the levels of p-AKT, p-mTOR, p-p38 and p-ERK were unchanged (Fig. 7A). At the same time, we found that after miR-25-3p inhibition, the levels of p15, cytoplasmic FOXO3 and nuclear FOXO3 were increased, but the phenomena were reversed after addition of FOXO pathway inhibitor AS1842856 (Fig. 7B), demonstrating that miR-25-3p could suppress FOXO pathway. Moreover, we found that miR-25-3p could combine with FOXO3 through ENCORI website (Table S4), and FOXO3 expression was elevated after inhibiting miR-25-3p expression (Fig. 7C). The binding sites between miR-25-5p and BAMBI 3'UTR were obtained and listed in Fig. 7D. Additionally, we proved that miR-25-3p could bind to FOXO3 3'UTR by measuring the weakened luciferase activity of pmirGLO reporter vector containing the whole sequence of FOXO3-3'UTR under miR-25-3p overexpression (Fig. 7E). Furthermore, RNA pull-down assay further demonstrated that miR-25-3p was only enriched in the products pulled down by Bio-FOXO3 3' UTR (Fig. 7F). Finally, we overexpressed FOXO3 (Fig. 7G) and found that he reduced levels of p15 and p19 caused by miR-25-3p overexpression were enhanced again after overexpression of FOXO3 (Fig. 7H).

BAMBI and FOXO3 jointly involves in HNRNPA2B1-mediated PCa cell apoptosis and migration

We also identified the effects of HNRNPA2B1 and CSNK1D on the activity of TGF-β signaling pathway and FOXO signaling pathway. As shown in Figure S2A–S2B, silencing of HNRNPA2B1 or CSNK1D could decrease the protein levels of p-SMAD2 and p-SMAD3 but had opposite effects on FOXO3 and p15. Subsequently, we conducted rescue assays to make a conclusion. Before that, BAMBI and FOXO3 was separately silenced in two PCa cells (Fig. 8A). As detected by flow cytometry and TUNEL assay, apoptosis rate enhanced by HNRNPA2B1 knockdown was partially reduced by the silencing of BAMBI or FOXO3 but was totally reduced to the original level by silencing of both BAMBI and FOXO3 (Fig. 8B, C). Additionally, cell migration suppressed by HNRNPA2B1 knockdown was partially recovered by the silencing of BAMBI or FOXO3 but was totally rescued by silencing of both BAMBI and FOXO3 (Fig. 8D, E).

Taken together, this study demonstrated that CSNK1D protein can bind to HNRNPA2B1 protein and mediate the phosphorylation of HNRNPA2B1 protein to enhance its protein stability. HNRNPA2B1 promotes the maturation of miR-25-3p/miR-93-5p by recognizing the m6A site and facilitates the malignant processes of PCa cells by activating BAMBI-mediated TGF-β signaling pathway and inactivating FOXO3-mediated FOXO signaling pathway (Fig. 9).

Discussion

Increasing evidences have indicated the important role of HNRNPA2B1 in tumor progression. For example, HNRNPA2B1 regulates tamoxifen- and fulvestrant-sensitivity and hallmarks of endocrine resistance in breast cancer cells [22]; HNRNPA2B1 promotes epithelial–mesenchymal transition in pancreatic cancer cells through ERK/snail signaling pathway [23]; HNRNPA2B1 promotes the proliferation of breast cancer cells via the STAT3 pathway [24]. In our study, we proved that HNRNPA2B1 promotes the malignant processes of PCa cells both in vitro and in vivo.

The m^6A modification is a newly founded RNA modification-mediated epigenetic regulation, which is closely linked to gene expression and cancer development [25]. Usually, m^6A modification is modulated via the methyltransferases and demethylases [26]. The m^6A "readers" can recognize m^6A-modified sites and affect RNA fate [27]. Many literatures have indicated that m^6A modification and its modulators play important parts in PCa. For instance, METTL3 promotes the progression of PCa via m^6A-modified LEF1 [28]; YTHDF2 accelerates PCa progression via mediating the mRNA degradation of LHPP and NKX3-1 in m^6A-dependent way [29]. Moreover, a previous study has unveiled that the m^6A reader HNRNPA2B1 promotes esophageal cancer progression via regulating ACLY and ACC1 [30], but its m^6A modification in PCa has not been systematically reported yet. As a nuclear m^6A reader, HNRNPA2B1 can regulate alternative splicing of nuclear RNAs containing RGm6AC sites [31]. Furthermore, HNRNPA2B1 promotes the processing of pri-miRNAs in a m6A-dependent manner [32]. In our study, we screened out the miRNAs associated with HNRNPA2B1 by analyzing data from TCGA database.

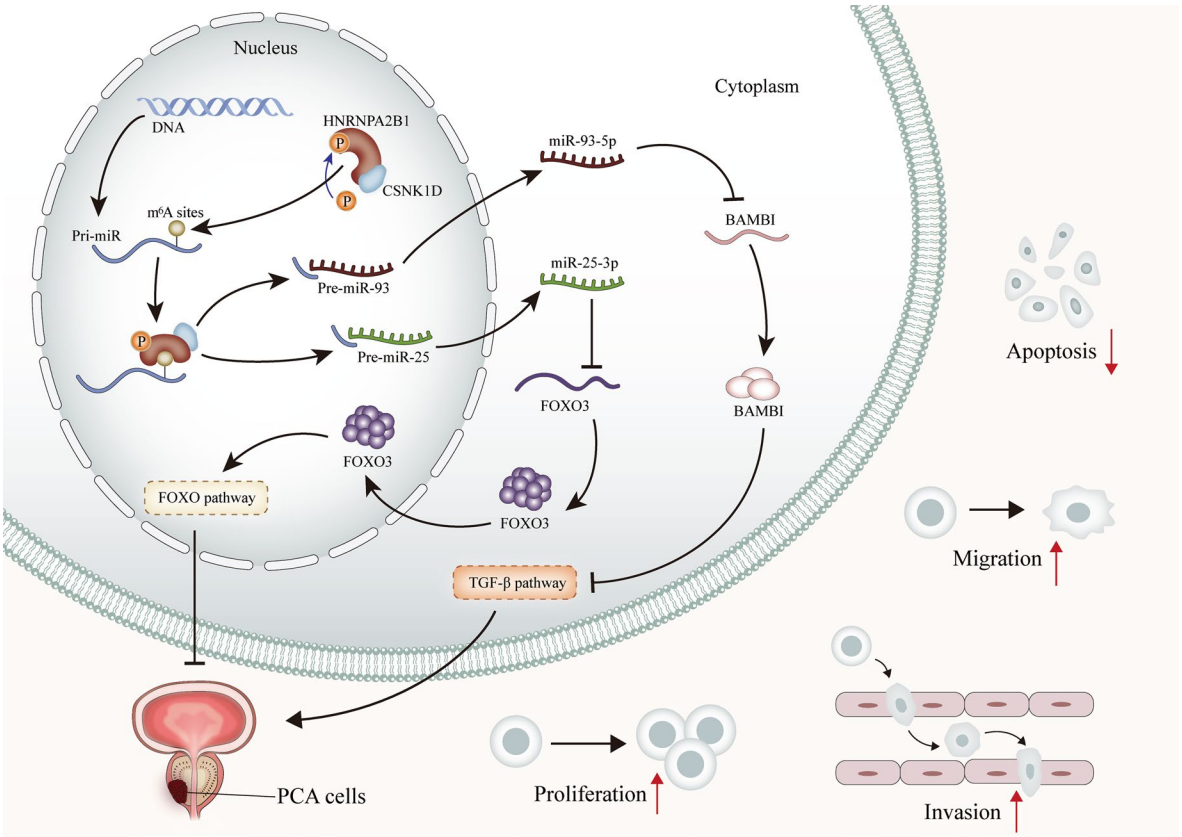

Fig. 9 A schematic plan showing the mechanism of HNRNPA2B1 functioning in the malignant processes of PCa cells

Our study firstly proposed that HNRNPA2B1 induced miR-25-3p/miR-93-5p maturation by recognizing the m^6A sites in PCa cells. In addition, our study found that HNRNPA2B1 could interact with CSNK1D in PCa cells. CSNK1D is a casein kinase which has been reported to phosphorylate PER2 and enhance its stability [33]. Consistently, our study also confirmed that CSNK1D phosphorylated HNRNPA2B1 at threonine 20 site and therefore stabilized HNRNPA2B1 protein.

Several studies have shown that miR-25-3p acts as an oncogenic miRNA in many cancers, such as osteosarcoma [34], glioma [35] and retinoblastoma [36]. Consistently, our study found that miR-25-3p was up-regulated in PCa cells. Moreover, our data revealed that miR-25-3p promoted cell migration and suppressed cell apoptosis in PCa. As demonstrated by a previous study, miR-25-3p affects esophageal cancer progression via regulation of PI3K/AKT pathway [37]. FOXO3 is a forkhead transcription factor with a distinct forkhead domain and a key protein in the FOXO pathway. Besides, FOXO3 has been documented to inhibit PCa progression [38]. At the same time, it has been reported that activation of FOXO signaling pathway in the nucleus inhibits the progression of PCa [39]. In the present study, we first put forward that miR-25-3p inactivated the FOXO pathway via targeting FOXO3 to promote PCa cell growth and migration. Moreover, miR-93-5p has been demonstrated to promote PCa cell migration, and it can also promote cancer progression via regulation of signaling pathways such as Hippo signaling pathway [40], STAT3 signaling pathway [41] and PI3K/AKT signaling pathway [42]. In our study, we found that miR-93-5p promoted PCa cell migration and inhibited apoptosis via activating TGF-β pathway. It has been reported that the activation of TGF-β signaling pathway promotes the progression of PCa [43]. BAMBI is a negative, competitive pseudo receptor for TGFβ and the subsequent Smad signaling pathways. Our study proved that miR-93-5p activated TGF-β pathway by inhibiting BAMBI expression.

The androgen receptor (AR) signaling pathway plays a crucial role in the occurrence and progression of PCa. Its ligand (dihydrotestosterone) binds to AR to induce its activation and then enters the nucleus. In the nucleus, AR binds to the androgen response element ARE (androgen response element), which in turn plays a role as a transcription activator and promotes biological functions such as tumor cell proliferation and invasion. We explored the expression correlation between AR and HNRNPA2B1 or CSNK1D in the TCGA database. Results showed that AR expression was

significantly positively correlated with the expression of HNRNPA2B1 and CSNK1D in PCa tissues (Figure S3A-B). The correlation between the expression of AR and HNRNPA2B1 and CSNK1D also indicated that the findings of our study might have a potential connection with AR. In future research, we will further explore the relevant mechanisms to enrich the theoretical basis for the malignant progression of PCa.

In conclusion, our study provided evidences that CSNK1D-phosphorylated HNRNPA2B1 promoted PCa progression via inducing the maturation of miR-25-3p/miR-93-5p by m^6A-dependent way. All these findings indicated that HNRNPA2B1 may be a promising prognostic biomarker and therapeutic target for PCa. However, many mechanisms in this regulation process remain unclear, and further studies are needed to support this theoretical model in the future.

Supplementary Information The online version contains supplementary material available at https://doi.org/10.1007/s00018-023-04798-5.

Author contributions XL and CQ designed the study and reviewed the data. FQ and WYS performed experiments and drafted the manuscript. XYW and YFC performed bioinformatics analyses. All the authors have read, revised, and approved the manuscript.

Funding This work was supported by grants from Young Talents Program of Jiangsu Cancer Hospital (No. 2017YQL-04), and The Research Project of Jiangsu Cancer Hospital (ZM202015).

Data availability The datasets used and/or analyzed during the current study are available from the corresponding author on reasonable request.

Declarations

Conflict of interest The authors declare no conflict of interests.

Ethics approval This study was approved by the Institutional Review Board of the First Affiliated Hospital of Nanjing Medical University.

Consent to participate All patients participating in the study voluntarily donated samples for clinical research and signed a consent form before surgery.

Consent to publish The authors affirm the research consent for publication.

References

1. Siegel RL, Miller KD, Jemal A (2019) Cancer statistics, 2019. CA Cancer J Clin 69:7–34
2. Teo MY, Rathkopf DE, Kantoff P (2019) Treatment of advanced prostate cancer. Annu Rev Med 70:479–499
3. Dai D, Wang H, Zhu L, Jin H, Wang X (2018) N6-methyladenosine links RNA metabolism to cancer progression. Cell Death Dis 9:124
4. Wang X, Lu Z, Gomez A et al (2014) N6-methyladenosine-dependent regulation of messenger RNA stability. Nature 505:117–120
5. Wu B, Su S, Patil DP et al (2018) Molecular basis for the specific and multivariant recognitions of RNA substrates by human hnRNP A2/B1. Nat Commun 9:420
6. Alarcón CR, Goodarzi H, Lee H et al (2015) HNRNPA2B1 is a mediator of m(6)A-dependent nuclear RNA processing events. Cell 162:1299–1308
7. Gupta A, Yadav S, Pt A et al (2020) The HNRNPA2B1-MST1R-Akt axis contributes to epithelial-to-mesenchymal transition in head and neck cancer. Lab Invest 100:1589–1601
8. Yang Y, Wei Q, Tang Y et al (2020) Loss of hnRNPA2B1 inhibits malignant capability and promotes apoptosis via down-regulating Lin28B expression in ovarian cancer. Cancer Lett 475:43–52
9. Hu Y, Sun Z, Deng J et al (2017) Splicing factor hnRNPA2B1 contributes to tumorigenic potential of breast cancer cells through STAT3 and ERK1/2 signaling pathway. Tumour Biol 39:1010428317694318
10. Stockley J, Villasevil ME, Nixon C et al (2014) The RNA-binding protein hnRNPA2 regulates β-catenin protein expression and is overexpressed in prostate cancer. RNA Biol 11:755–765
11. Ji G, Huang C, He S et al (2020) Comprehensive analysis of m6A regulators prognostic value in prostate cancer. Aging (Albany NY) 12:14863–14884
12. Tutar L, Özgür A, Tutar Y (2018) Involvement of miRNAs and pseudogenes in cancer. Methods Mol Biol 1699:45–66
13. Alarcón CR, Lee H, Goodarzi H, Halberg N, Tavazoie SF (2015) N6-methyladenosine marks primary microRNAs for processing. Nature 519:482–485
14. Lu TX, Rothenberg ME (2018) MicroRNA. J Allergy Clin Immunol 141:1202–1207
15. Fabris L, Ceder Y, Chinnaiyan AM et al (2016) The potential of MicroRNAs as prostate cancer biomarkers. Eur Urol 70:312–322
16. Zi Z (2019) Molecular engineering of the TGF-β signaling pathway. J Mol Biol 431:2644–2654
17. Thakur N, Hamidi A, Song J, et al. (2020) Smad7 enhances TGF-β-induced transcription of c-jun and HDAC6 promoting invasion of prostate cancer cells. iScience 23**:**101470.
18. Link W (2019) Introduction to FOXO biology. Methods Mol Biol 1890:1–9
19. Yan Y, Huang H (2019) Interplay among PI3K/AKT, PTEN/FOXO and AR signaling in prostate cancer. Adv Exp Med Biol 1210:319–331
20. Xu J, Chen Q, Tian K et al (2020) m6A methyltransferase METTL3 maintains colon cancer tumorigenicity by suppressing SOCS2 to promote cell proliferation. Oncol Rep 44:973–986
21. Chava S, Reynolds CP, Pathania AS et al (2020) miR-15a-5p, miR-15b-5p, and miR-16-5p inhibit tumor progression by directly targeting MYCN in neuroblastoma. Mol Oncol 14:180–196
22. Petri BJ, Piell KM, South Whitt GC et al (2021) HNRNPA2B1 regulates tamoxifen- and fulvestrant-sensitivity and hallmarks of endocrine resistance in breast cancer cells. Cancer Lett 518:152–168
23. Dai S, Zhang J, Huang S et al (2017) HNRNPA2B1 regulates the epithelial-mesenchymal transition in pancreatic cancer cells through the ERK/snail signalling pathway. Cancer Cell Int 17:12
24. Gao LB, Zhu XL, Shi JX et al (2021) HnRNPA2B1 promotes the proliferation of breast cancer MCF-7 cells via the STAT3 pathway. J Cell Biochem 122:472–484
25. Liu ZX, Li LM, Sun HL, Liu SM (2018) Link between m6A modification and cancers. Front Bioeng Biotechnol 6:89
26. Coker H, Wei G, Brockdorff N (2019) m6A modification of non-coding RNA and the control of mammalian gene expression. Biochim Biophys Acta Gene Regul Mech 1862:310–318

27. Yang G, Sun Z, Zhang N (2020) Reshaping the role of m6A modification in cancer transcriptome: a review. Cancer Cell Int 20:353
28. Ma XX, Cao ZG, Zhao SL (2020) m6A methyltransferase METTL3 promotes the progression of prostate cancer via m6A-modified LEF1. Eur Rev Med Pharmacol Sci 24:3565–3571
29. Li J, Xie H, Ying Y et al (2020) YTHDF2 mediates the mRNA degradation of the tumor suppressors to induce AKT phosphorylation in N6-methyladenosine-dependent way in prostate cancer. Mol Cancer 19:152
30. Guo H, Wang B, Xu K et al (2020) m(6)A reader HNRNPA2B1 promotes esophageal cancer progression via up-regulation of ACLY and ACC1. Front Oncol 10:553045
31. Chen XY, Zhang J, Zhu JS (2019) The role of m(6)A RNA methylation in human cancer. Mol Cancer 18:103
32. Klinge CM, Piell KM, Tooley CS, Rouchka EC (2019) HNRNPA2/B1 is upregulated in endocrine-resistant LCC9 breast cancer cells and alters the miRNA transcriptome when overexpressed in MCF-7 cells. Sci Rep 9:9430
33. Eng GWL, Edison VDM (2017) Site-specific phosphorylation of casein kinase 1 δ (CK1δ) regulates its activity towards the circadian regulator PER2. PLoS One 12:e0177834
34. Rao HC, Wu ZK, Wei SD et al (2020) MiR-25-3p serves as an oncogenic MicroRNA by downregulating the expression of merlin in osteosarcoma. Cancer Manag Res 12:8989–9001
35. Peng G, Yang C, Liu Y, Shen C (2019) miR-25-3p promotes glioma cell proliferation and migration by targeting FBXW7 and DKK3. Exp Ther Med 18:769–778
36. Wan W, Wan W, Long Y et al (2019) MiR-25-3p promotes malignant phenotypes of retinoblastoma by regulating PTEN/Akt pathway. Biomed Pharmacother 118:109111
37. Zhang L, Tong Z, Sun Z, et al. (2020) MiR-25–3p targets PTEN to regulate the migration, invasion, and apoptosis of esophageal cancer cells via the PI3K/AKT pathway. Biosci Rep 40
38. Kong Z, Deng T, Zhang M et al (2018) β-arrestin1-medieated inhibition of FOXO3a contributes to prostate cancer cell growth in vitro and in vivo. Cancer Sci 109:1834–1842
39. Shan Z, Li Y, Yu S et al (2019) CTCF regulates the FoxO signaling pathway to affect the progression of prostate cancer. J Cell Mol Med 23:3130–3139
40. Li L, Zhao J, Huang S et al (2018) MiR-93-5p promotes gastric cancer-cell progression via inactivation of the Hippo signaling pathway. Gene 641:240–247
41. Ma DH, Li BS, Liu JJ et al (2017) miR-93-5p/IFNAR1 axis promotes gastric cancer metastasis through activating the STAT3 signaling pathway. Cancer Lett 408:23–32
42. Cao Y, Xia F, Wang P, Gao M (2018) MicroRNA-93-5p promotes the progression of human retinoblastoma by regulating the PTEN/PI3K/AKT signaling pathway. Mol Med Rep 18:5807–5814
43. Li Y, Zhang B, Xiang L et al (2020) TGF-β causes Docetaxel resistance in Prostate Cancer via the induction of Bcl-2 by acetylated KLF5 and Protein Stabilization. Theranostics 10:7656–7670